Polymer Testing 68 (2018) 415–423

Contents lists available at ScienceDirect

Polymer Testing

journal homepage: www.elsevier.com/locate/polytest

Material Properties

Interlaminar bonding performance of 3D printed continuous fibre reinforced thermoplastic composites using fused deposition modelling

M.A. Caminero[a,*], J.M. Chacón[b], I. García-Moreno[a], J.M. Reverte[b]

[a] Escuela Técnica Superior de Ingenieros Industriales, INEI, Universidad de Castilla-La Mancha, Campus Universitario s/n, 13071, Ciudad Real, Spain
[b] Escuela Técnica Superior de Ingenieros Industriales, IMACI, Universidad de Castilla-La Mancha, Campus Universitario s/n, 13071, Ciudad Real, Spain

ARTICLE INFO

Keywords:
Fused deposition modelling
Continuous fibre reinforced thermoplastic composites
Interlaminar shear strength
Failure analysis

ABSTRACT

Continuous fibre reinforced thermoplastic composites (CFRTPCs) are becoming more significant in industrial applications due to their inherit advantages such as excellent mechanical performance, potential use in lightweight structures and being recyclable. Fused deposition modelling (FDM) is a promising additive manufacturing technology and an alternative to conventional processes for the fabrication of CFRTPCs due to its ability to build functional parts having complex geometries. However, a major concern affecting the efficient use of 3D printed composites is their weak interlaminar bonding performance compared to conventional pre-preg composites. The aim of this study is to evaluate the effect of layer thickness and fibre volume content on the interlaminar bonding performance of 3D printed continuous carbon, glass and Kevlar® fibre reinforced nylon composites manufactured by FDM technique. Short beam shear tests were carried out to determine interlaminar shear strength (ILSS). SEM images and cross-sectional micrographs were examined to assess failure mechanics of the different configurations.

It was observed that the effect of layer thickness of nylon samples on the interlaminar shear performance was marginally significance. ILSS values decrease as layer thickness increase due to higher porosity. In addition, continuous fibre reinforced samples show higher ILSS values than unreinforced ones but, conversely, the level of increase in ILSS is moderate with continued increase in fibre content, particularly in the case of Kevlar® fibre. Carbon fibre reinforced composites exhibit the best interlaminar shear performance with higher stiffness. On the other hand, Kevlar® fibre reinforced composites have the lowest interlaminar shear performance due to poor wettability of Kevlar® fibre bundles by the nylon, leading to extensive delamination. Finally, the results obtained demonstrate that it is still a challenge to increase shear performance of 3D printed composites with respect to common pre-preg materials. Nevertheless, ILSS values exhibited by 3D printed composites are significantly higher than the usual 3D printed thermoplastics.

1. Introduction

Additive manufacturing (AM) technologies have found potential applications for creating complex lightweight structures in aerospace industries, architectural industries for structural models, art fields, education or medical fields for printing tissues and organs [1–6]. These technologies are able to accurately manufacture a large range of prototypes or functional components with complex geometries, such as those obtained from a topology optimization process [7,8] or generated from a fitting process in Computer-Aided Design [9], which are difficult, if not impossible, to manufacture using conventional methods [10–12]. Compared to these methods, AM technologies can shorten the design-manufacturing cycle, reduce production costs and increase competitiveness [4–6]. AM technology is a very broad term encompassing numerous methods such as Stereolithography (STL) of a photopolymer liquid, Fused Deposition Modelling (FDM) from polymer filaments, Laminated Object Manufacturing (LOM) from plastic laminations, and Selective Laser Sintering (SLS) from plastic or metal powders [2,13]. However, the FDM technique is of particular interest due to its relative low cost, low material wastage and ease of use [1]. FDM forms a 3D geometry through the deposition of successive layers of extruded thermoplastic filament, such as acrylonitrile butadiene styrene (ABS), polylactic acid (PLA), polypropylene (PP) or polyethylene (PE). Engineering thermoplastics with improved mechanical performance, such as polyamide (PA or Nylon), polycarbonate (PC), polyetheretherketone (PEEK), polyetherimide (PEI), polyethersulfone (PES) or polyphenylene sulfide (PPS) are also available [14]. Due to this process, delamination of the component layers can occur resulting in

* Corresponding author.
E-mail address: miguelangel.caminero@uclm.es (M.A. Caminero).

https://doi.org/10.1016/j.polymertesting.2018.04.038
Received 14 March 2018; Accepted 24 April 2018
Available online 27 April 2018

premature failure. Additionally, FDM printed parts typically have lower elastic properties than injection moulded components of the same thermoplastic [2].

FDM has started to move beyond its initial role as prototyping technology to a process that can build finished parts. However, most of 3D printed polymer products are still used as conceptual prototypes rather than functional components, since pure polymer products built by FDM lack strength and functionality [15–17]. Furthermore, mechanical properties of parts fabricated by conventional FDM 3D printing are inherently poor because of the thermoplastic resin used, although the optimization of processing parameters, such as build orientation, layer thickness or feed rate, has been investigated for improving the mechanical properties of thermoplastic parts [1,3,18,19]. Furthermore, enhanced thermoplastic matrix, such as PEEK or PEI, have been analysed to improve the mechanical performance and thermal applicability of FDM structures [20–23]. Such drawbacks restrict the wide industrial application of 3D printed thermoplastic polymers, leaving prototyping as the primary application [15].

However, in the last decade, there has been an increasing interest in introducing these technologies in the manufacturing of primary structural parts. 3D printing of polymer composites with enhanced mechanical properties solves the previous limitations by combining the matrix and reinforcements to achieve a system with more useful structural or functional properties non-attainable by any of the constituent alone [6,24]. Incorporation of particle, fibre or nanomaterial reinforcements into polymers permits the fabrication of polymer matrix composites that are characterized by high performance and excellent functionality [4,6,24]. Various reinforcement, such as short fibres, including chopped carbon fibres, carbon nanotubes or glass fibres have been used [5,10,23,26–29]. In most studies, the additives were mixed into thermoplastic filaments prior to being loaded into the printer. However, these composites show poor mechanical properties compared to composites manufactured by conventional methods because composites reinforced with short fibres or particles are mechanically lower than composites reinforced with continuous fibres. The possibility of employing continuous reinforced fibres, such as carbon, aramid or glass, may lead to product with much higher mechanical performance which are potentially useful for advanced applications [30]. CFRTPCs are becoming alternative materials to replace the conventional thermosetting polymers and metals due to excellent mechanical performance, recycling and potential lightweight structures. FDM is a promising alternative of conventional processes for the fabrication of CFRTPCs, such as vacuum forming, filament winding, pultrusion, bladder-assisted moulding or compression, that require expensive facilities and equipment, such as autoclaves or complex rigid moulds for out-of-autoclave processes, hindering the wide application of composites [14,31,32].

To date, continuous fibre reinforced 3D printed thermoplastic filaments, as the feedstock of FDM process, have not been extensively investigated in literature [5,6,25]. For the FDM case, two possibilities for embedding the continuous reinforced fibres into thermoplastic filament have been considered in the literature: embedding the continuous fibre directly in the component with a dual extrusion method [2,15,17,24], or embedding the continuous fibre in the injector in a “co-extrusion” process [16,25,32,33]. The previous studies have highlighted the impact of different process parameters, such as layer thickness, fibre volume fraction, fibre placement or fibre orientation on the mechanical performance of FDM parts under tensile and flexural loading. Different combinations of fibre reinforcements and thermoplastic matrix have been analysed: continuous carbon, glass or Kevlar® fibre reinforcements embedded in PLA, ABS or Nylon thermoplastic matrix [4–6]. The results of the previous studies have shown an increase in mechanical strength of continuous fibre reinforced 3D printed composite structures compared to pure thermoplastic 3D printed structures. However, the level of increase in strength was moderated with continued increase in fibre content due to weak bonding between the fibre/matrix layers, as well as the presence of increased levels of air voids (porosity) with fibre content [5,15]. Remarkable improvement in mechanical performances of 3D printed composites are claimed by the MarkForged® Company [34], which employs a method involving the dual extrusion of a continuous fibre reinforced composite filament; in this case, specific filaments in the form of tow of fibres for the manufacturing of nylon composites are deposited with a specially designed printer [2,15,17,24,30].

Hence, using FDM to fabricate CFRTPCs components with much higher mechanical performance has become a cutting-edge and interdisciplinary research topic in the last few years. Among the existing literature on mechanical properties of 3D printed composite polymers, there is a lack of study on the interlaminar bonding behaviour [32,35]. Interlaminar matrix regions between the reinforced fibres layers are critical regions that are highly susceptible to delamination under mechanical loading. Delamination may be a result of weak matrix, bad layup or mechanical loading type, and it often introduces internal damage in composites which could potentially result in the global failure of a component with reduced strength and stiffness [36]. Furthermore, porosity and weak interface bonding between fibres and matrix have been cited as a major concern for 3D printed fibre reinforced polymer composites [37]. The interface bonding quality between layers and wires significantly influences the microstructure and mechanical properties of the resulting parts.

In this study, interlaminar bonding performance of 3D printed continuous fibre reinforced composites manufactured by FDM technique was evaluated by means the short beam shear (SBS) test [38] to obtain the interlaminar shear strength (ILSS). The MarkForged® MarkTwo [34] system was used for the manufacture of nylon ILSS composite samples with carbon, glass and Kevlar® fibres as reinforcements. The effects of two process parameters, namely, layer thickness and fibre volume fraction are particularly analysed. A comparison of the interlaminar bonding performance between virgin and reinforced printed samples was conducted. Finally, optical micrographs and SEM images of the failure surfaces of ILSS samples were evaluated to determine the effects of process parameters on the interlaminar bonding quality.

The rest of the paper is organized as follows. First, the experimental methodology used is briefly summarized with particular emphasis on specimen preparation, 3D printing process and the experimental set-up. Thereafter, the key results of the investigation are summarized and the effects of the different process parameters are highlighted. Finally, conclusions and extensions of this work are outlined.

2. Experimental methodology

2.1. Materials, 3D printer and specimen preparation

The goal of this study is to analyse the interlaminar bonding strength of 3D printed CFRTPCs samples using two different process parameters: layer thickness and fibre volume fraction. Nylon filament (matrix) was supplied by Markforged® with a diameter of 1.75 mm. Prior to use, this thermoplastic polymer was stored in a Pelican® 1430 modified dry box to minimize moisture absorption in the same way as the manufactured test specimens prior to testing [1]. The fibres, glass, carbon and Kevlar® fibre were also supplied by Markforged®. The fibres were composed of bundles infused with a sizing agent. Fibre bundles of carbon were 0.35 mm in diameter and Kevlar® and glass were 0.3 mm. The basic stiffness and strength properties of nylon and continuous fibres used in this study are depicted in Table 1. In addition, the main mechanical properties of PLA and ABS materials manufactured by FDM technology [1,11,13], are included for comparative purposes.

3D printed CFRTPCs samples were manufactured using a MarkForged® MarkTwo desktop 3D printer. The printing process consists of two stages, each of which is performed by a separate print head. This system can print two kinds of material independently and, hence, it has two extruders and two print heads (Fig. 1). One of the print heads is

Table 1
Stiffness and Strength properties of the nylon matrix and continuous fibres. Typical ranges of mechanical properties of PLA and ABS materials fabricated by FDM technology are also included for comparative purposes.

Properties	Nylon	Carbon	Glass	Kevlar®	PLA	ABS
Tensile Strength (MPa)	31	700	590	610	15.5–72.2	36–71.6
Tensile Modulus (MPa)	940	54000	21000	27000	2020–3550	99.8–2413
Elongation at Break (%)	54	1.5	3.8	2.7	0.5–9.2	3–20
Flexural Strength (MPa)	32	470	210	190	52–115.1	48–110
Flexural Modulus (MPa)	840	51000	22000	26000	2392–4930	1917–2507

used to print nylon (matrix) and the other is used to print fibre reinforcement. Nylon and fibre layers were printed with hot end temperatures of 273 °C and 232 °C, respectively, on a non-heated print bed. Carbon fibre was printed in layers of 0.125 mm, while Kevlar® and glass fibres were printed in layers of 0.1 mm. The design of the 3D printer allows continuous fibre reinforcement to be placed as required. It allows specifying the fibre orientation on the layer-by-layer deposition process. MarkTwo uses its own software designated Eiger®. This software allows importing .STL and .OBJ models.

There is no standard test method for determine the interlaminar shear strength (ILSS) properties of parts manufactured using FDM. In this work, the ISO 14130 [38] method was applied for the analysis of the interlaminar shear performance. The geometry of the 3D printed specimens was modelled using SolidWorks software, exported as an STL file and imported to the 3D printing software. Two types of fibre pattern can be selected in the MarkForged® MarkTwo desktop 3D printer: concentric and isotropic. In this study, isotropic fibre patterns were analysed. The isotropic fibre pattern consists of parallel lines, with areas without fibre filled by nylon, before the subsequent layer is printed. The term isotropic does not define the mechanical properties of the test specimens. Isotropic fill is in this case resulted in unidirectional anisotropic specimens. Furthermore, the isotropic pattern was observed to yield higher tensile strength and stiffness than concentric pattern [15]. ILSS samples were obtained from a 3D printed panel (Fig. 2a) and cut later to avoid edge effects due to low fibre content areas filled by nylon. The main dimensions of the 3D printed panel and the ILSS specimens are shown in Fig. 2a.

2.2. Process parameters

The mechanical properties of parts fabricated using FDM technologies depend on the selection of process parameters [1] [6], [39]. Table 2 outlines the FDM printing parameters of the Markforged® MarkTwo 3D printer analysed in this study. Two types of specimens were considered: unreinforced and continuous reinforced nylon specimens. Three different layer thickness were assessed for the unreinforced nylon specimens: $L_t = \{0.1, 0.125, 0.2\}$ mm, and two different layer thickness were used for continuous reinforced specimens: $L_t = 0.125$ mm for carbon fibres and $L_t = 0.1$ mm for glass and Kevlar® fibres. The usual minimum layer thickness found in the literature was $L_t = 0.1$ mm [1].

In addition, two different fibre volume fractions were considered: partially reinforced and fully reinforced ILSS specimens. For ease of reference purposes, partially and fully reinforced ILSS specimens are labelled as “A” and “B”, respectively (Fig. 2b). Fibre volume fraction was estimated from averaged volume data reported by Eiger® software (Table 2). At least two nylon layers must be added in each specimen (roof and floor layers). The averaged fibre volume fraction of type A was 27.2% and type B was 73.2%. Furthermore, type A layered sequence was selected to maximize the mechanical performance of the ILSS specimens. These fibre volume fraction types helped to assess the effect of the fibre content (fibre layers) on the interlaminar shear strength and gained an insight into the interface bonding response of fibre layer-matrix layer contact (type A) and fibre layer-fibre layer contact (type B). Fig. 2c depicts SEM images showing details of the interfaces between fibre bundles and matrix (nylon) and the individual fibres (carbon fibre, glass fibre and Kevlar® fibre) within these bundles (~1000 fibres in each bundle).

Certain parameters, such temperature, feed rate, fill density and pattern of the thermoplastic matrix (nylon) and fibre angle or fibre fill

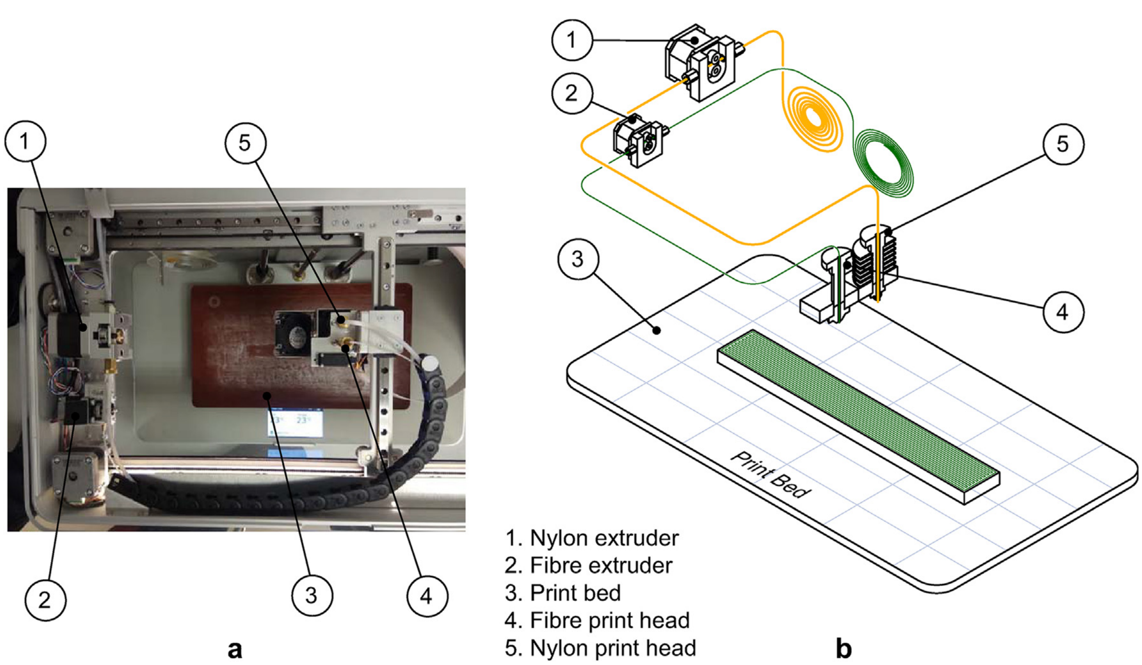

Fig. 1. Mark Two composite 3D printer system. (a) General view of the MarkForged® Mark Two desktop 3D printer. (b) Details of the printing process. The system has two separate extruders and print heads, one for the continuous fibre and one for the nylon (matrix), allowing the manufacture of continuous fibre composites using the FDM technique.

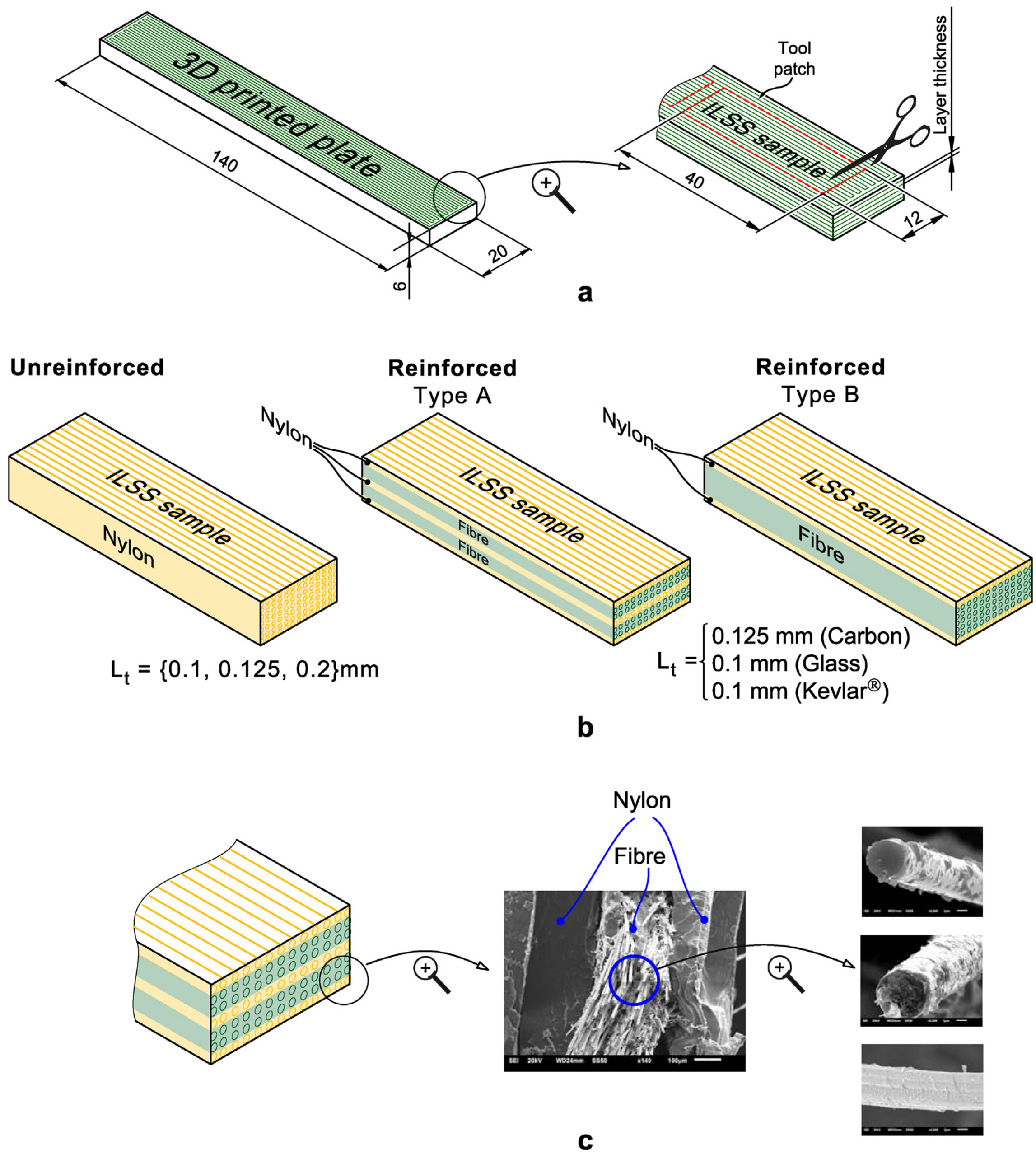

Fig. 2. Standard specimen for ILSS testing and process parameters. (a) Dimensions of the 3D printed reinforced panel (left) used to extract the ILSS samples (right). (b) Layer thickness (L_t) and fibre volume content (Type A and Type B). (c) SEM images showing details of the fibre bundles and individual fibres (carbon fibre, glass fibre and Kevlar® fibre).

Table 2
Printing parameters and their levels used in this work.

Parameter	Value	
Layer thickness of unreinforced samples (mm) (Number of layers)	L_t = {0.1(60), 0.125(48), 0.2(30)}	
Layer thickness of fibre reinforced samples (mm)	$L_t^{CARBON} = 0.125$, $L_t^{GLASS} = L_t^{KEVLAR} = 0.1$	
Fibre volume fraction (%) (Number of fibre layers/Number of layers)	**Fibre volume type**	
	Type A	Type B
	Carbon fibre	
	26.8 (18/48)	72.4 (46/48)
	Kevlar® fibre	
	27.5 (22/60)	73.8 (58/60)
	Glass fibre	
	27.2 (22/60)	73.4 (58/60)

Table 3
Fixed parameters.

Print parameters	Value
Unreinforced samples	
Fill density (%)	100
Fill pattern	Rectangular
Reinforced samples	
Fibre fill type	Isotropic
Fibre angle	0°

type (isotropic) were fixed for all the samples to focus on the influence of the previous parameters (Table 3).

2.3. Experimental set-up

Each sample set consisted of five specimens for a given group of process parameters. Average interlaminar shear strength values of the mechanical test were taken as the results. Since the physical properties of many materials (especially thermoplastics) can vary depending on ambient temperature, tests were carried out at room temperature.

Dimensions of the SBS specimens were selected such that the span length = thickness x 4 and width = thickness x 2. A 50 kN universal electro-mechanical testing machine with a 5 kN load cell at a fixed loading rate of 1 mm/min was used for the SBS tests. The experimental data were processed following the recommendations of the standard for the determination of the interlaminar shear strength as

$$\tau_{ILSS} = 0.75 \times \frac{P_m}{b \times h}$$

where τ_{ILSS} is the interlaminar shear strength (ILSS), P_m is the maximum load observed during and the test, b is the width of the specimen and h the thickness of the specimen.

3. Results and discussion

Average and standard deviation of the test results of the maximum interlaminar shear strength (τ_{ILSS})are tabulated for the unreinforced nylon ILSS samples in Table 4 and for reinforced nylon ILSS samples in Table 5.

In order to clarify the results for a better understanding of the correlation between the different ranges of process parameters on interlaminar bonding performance, a graphical representation of these results is shown in Fig. 3.

This figure shows the average interlaminar shear strength as a function of the layer thickness and fibre volume fraction (Fig. 3a and b). In addition, the bonding performance in terms of interlaminar shear strength of continuous reinforced nylon composites have been compared with other common 3D printed thermoplastic and pre-preg composites (thermoset-matrix composite) manufactured with vacuum bag and autoclave (Fig. 3c). Finally, Fig. 4 reports some representative interlaminar shear strength-displacement curves and failure modes for the ILSS samples with different process parameters to characterise and assess different types of damage observed. The main effects of the process parameters on the interlaminar bonding performance of 3D printed samples are summarized in the following sections.

3.1. Effect of layer thickness on the interlaminar bonding performance of unreinforced nylon specimens

Layer thickness is directly related to the number of layers needed to print a part and hence to printing time. Thus, manufacturing costs decrease as layer thickness increases. The effect of layer thickness on bonding performance of unreinforced nylon samples is illustrated in Figs. 3a and 4a. A first glance at these results reveal that the effect of layer thickness on the ILSS values of nylon samples was marginally significance (Table 4). Nevertheless, the results showed a slight decreasing trend of ILSS as the layer thickness increased, which it is in good agreement with the trends observed for tensile and flexural behaviour found in previous works [1,10,11]. Fig. 3a depicts SEM images of unreinforced ILSS samples showing details of the layer bonding (nylon-nylon layer contact) for different layer thickness. The thinner layers were found to facilitate overlap resulting in the filling of air voids by extra material extrusion and, hence, lower porosity and higher ILSS values. These results have confirmed the observations of previous studies [15,17,32][15,17,32]. In addition, Fig. 4a depicts ILSS-displacement curves and optical micrographs for the unreinforced nylon samples. The results highlighted ductile behaviour, with significant plastic deformation and high toughness.

Table 4
Average ILSS test results of unreinforced nylon samples and layer thickness ranges. Standard deviation is depicted in brackets.

Interlaminar shear strength of nylon samples τ_{ILSS} (MPa)		
L_t = 0.1 mm	L_t = 0.125 mm	L_t = 0.2 mm
10.19(0.25)	9.79(0.39)	9.33(0.38)

Table 5
Average ILSS test results of reinforced nylon samples and process parameters ranges. Standard deviation is depicted in brackets.

Interlaminar shear strength of reinforced nylon samples τ_{ILSS} (MPa)	
Fibre volume fraction	
Type A	Type B
Carbon fibre	
22.19(1.04)	31.94(1.89)
Kevlar® fibre	
13.65(0.57)	14.28(1.21)
Glass fibre	
13.87(1.42)	20.99(1.18)

3.2. Effects of type of fibre reinforcement and fibre volume fraction on the interlaminar bonding performance of reinforced nylon specimens

The bonding performance of the interface between fibres and matrix is a main factor for the mechanical strength of 3D printed composite parts. The maximum achievable strength of 3D printed fibre reinforced composites is limited by the fibre-matrix interaction in porous areas [6,15,32]. The role of the type of fibre reinforcement (carbon, glass or Kevlar®) and fibre volume fraction on the interlaminar bonding strength of 3D printed ILSS composite samples is analysed in this section. It is important to note that, during the printing procedure, no pressure was applied after a layer was laid up. It is well known that pressure plays a fundamental role on the manufacturing of laminated parts from both thermoset and thermoplastic-based composites. The absence of pressure in highly viscous matrices is directly related to the presence of defects (pores or matrix-dominated areas) [15,17]. Table 5 and Fig. 3b depict the average and standard deviation of the maximum ILSS values for the 3D printed reinforced nylon samples. Note that the scatter of the result is small, validating the obtained values. Two different fibre volume fractions were considered to study interface bonding between fibre/nylon layers: type A (27.2%, partially reinforced) and type B (73.2%, fully reinforced). The results reveal that the type of fibre reinforcement and fibre content significantly affected the interlaminar bonding performance of the 3D printed composite samples.

As demonstrated in Fig. 3b, an increase in ILSS was observed from unreinforced samples to 27,2% fibre volume fraction (type A) for the three reinforcements, with ILSS values increasing by 117% for carbon fibre samples (L_t = 0.125 mm) and 36% and 34% for glass and Kevlar® fibre samples (L_t = 0.1 mm), respectively. Fig. 4b shows the average ILSS-displacement behaviour and optical micrographs for the type A reinforced samples. In general, the results highlighted interlaminar shear failure due to delamination of the thermoplastic matrix as well as exfoliation between the reinforced fibres and the matrix (fibre-nylon bonding). In addition, the first interlaminar shear failure for the three reinforced samples occurred at a similar displacement level. However, carbon fibre reinforced samples depicted a more brittle behaviour due to higher stiffness (Table 1). Finally, SEM examination of the cross-

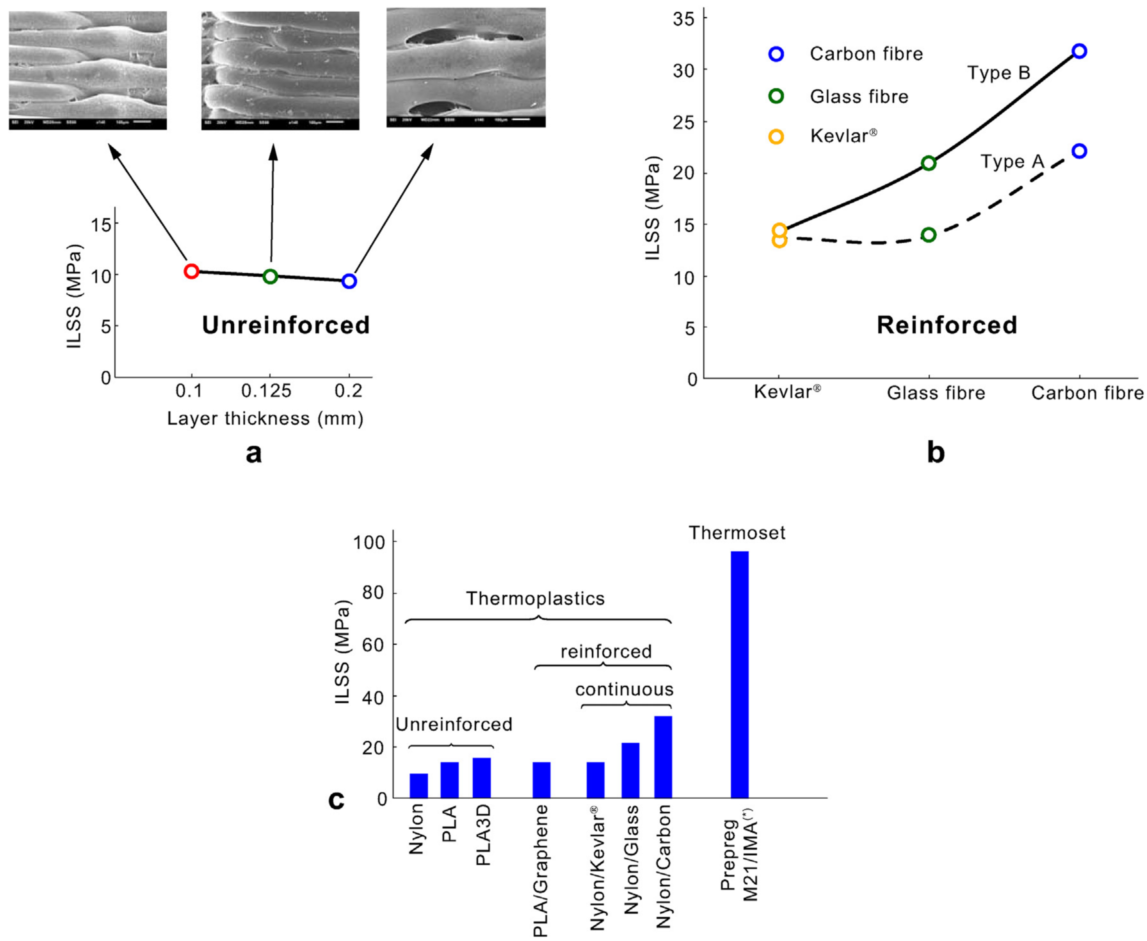

Fig. 3. Graphical comparison of average maximum interlaminar shear strength of ILSS specimens. (a) The effect of layer thickness in unreinforced ILSS samples. (b) The effect of fibre volume content. (c) Comparison of different 3D printed thermoplastic materials (unreinforced and reinforced) and pre-preg M21/IMA thermoset-matrix composite [40–42].

sectional ILSS samples was performed to obtain information on interlaminar shear failure mechanisms (Fig. 5). Fig. 5a depicts SEM images showing details of the interlaminar shear failure modes of type A samples. It is worth noting that carbon fibre reinforced samples exhibited fibre breakage and delamination, leading to higher ILSS values compared to glass and Kevlar® fibre reinforced samples.

Furthermore, increasing fibre content to 73.2% average fibre volume fraction (type B) resulted in a further increase to 213% for carbon fibre samples and 106% and 40% for glass fibre and Kevlar® fibre samples, respectively (Fig. 3b). These results indicated that this further increase in fibre content was not leading to a proportional increase in ILSS, except in the case of glass fibre samples. The likely explanation is air inclusions, that were observed to become larger and more frequent in the composite as the fibre content increased. This ingress of air is attributed to the atmospheric pressure environment in which the samples were fabricated. Conventional composites are typically manufactured at high pressures to remove major air inclusions. This porosity is a significant limitation for 3D printed composites and will clearly lead to significant strength loss compared to composites manufactured using conventional lay-up techniques. These results were in accordance with the observations reported in previous works [15,24,29]. Fig. 4c shows the average ILSS-displacement behaviour and optical micrographs for the type B reinforced samples. Carbon fibre reinforced samples depicted the best performance in terms of interlaminar shear strength and higher stiffness, with limited delamination due to interlaminar shear failure (Fig. 5b). However, glass and Kevlar® fibre reinforced samples showed more extensive delamination, particularly Kevlar® reinforced samples. The reasons of these different may be explained by the fibre/nylon interface bonding performance. Fig. 5c shows the poor wettability of Kevlar® fibre bundles by the nylon, the internal fibres were hardly infiltrated by the thermoplastic matrix and a limited number of external fibres could adhere to the matrix (nylon), suggesting a weaker bond to the nylon when compared to carbon and glass fibre bundles. This conclusion is supported by the occurrence of extensive shear failure, indicating that fibres are not consistently bonded to the matrix.

Finally, in order to study the use of 3D printed composite materials in functional applications, ILSS values of 3D printed continuous reinforced nylon composites have been compared with traditional 3D printed PLA samples, 3D printed graphene-reinforced PLA composites and conventional thermoset pre-preg composites manufactured with an autoclave (Fig. 3c). The prepreg material was M21/IMA carbon fibre/epoxy composite with 59,8% fibre volume fraction [40–42]. Note that this is a qualitative comparison, since the polymeric matrix and the fibres are different for 3D printing (thermoplastic) and pre-preg manufactured composites (thermoset). The comparison shows that the properties of 3D printed continuous reinforced composites are poor compared with conventional pre-preg materials. The reasons are the differences of the raw materials (matrix and fibres) compared with the epoxy matrix and carbon fibres of pre-preg composites and the manufacturing process itself, without any compaction stage between filament laid-up and even between layers (porosity).

Despite the poor properties of the 3D printed continuous reinforced composite material with respect to traditional pre-pegs composites, the

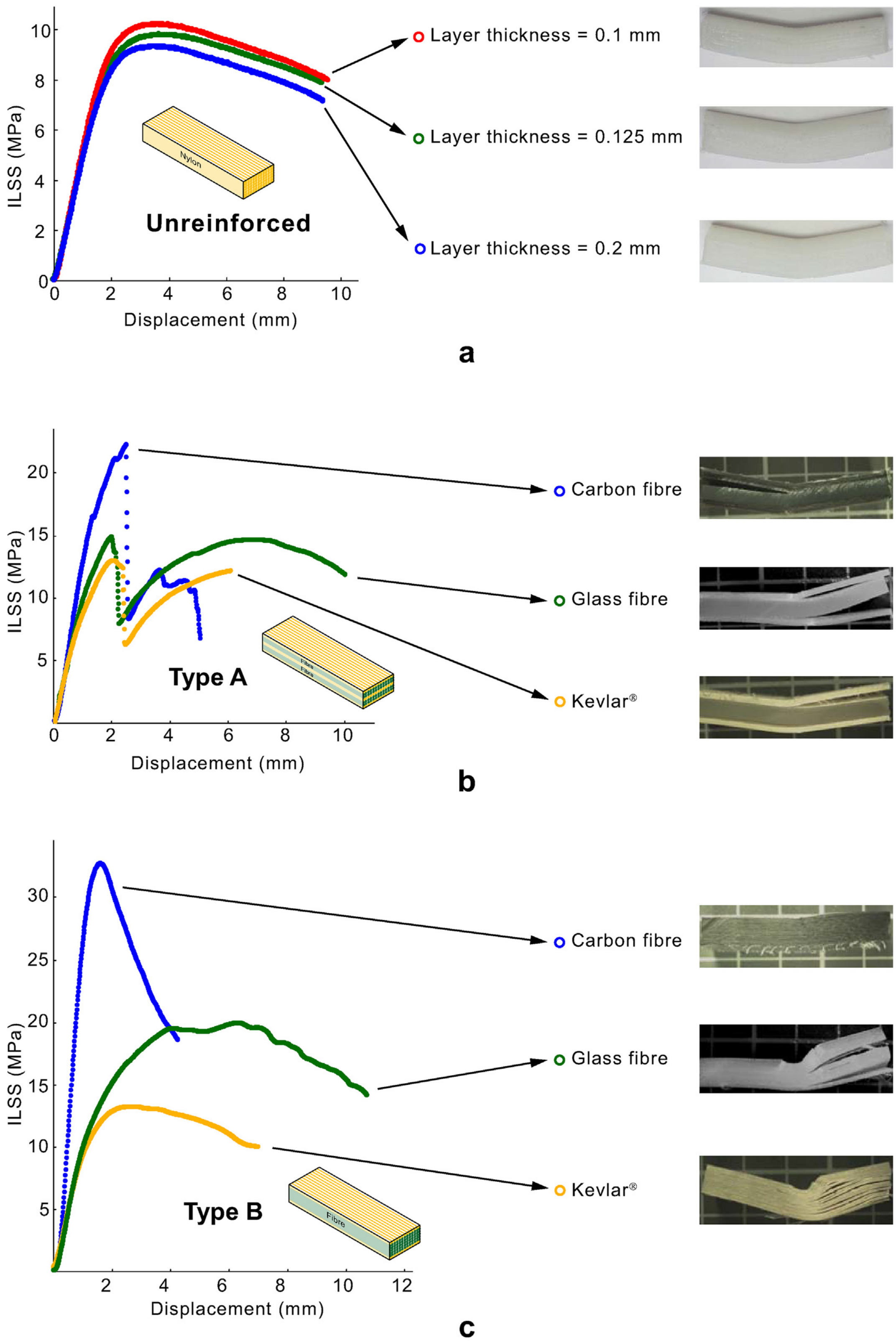

Fig. 4. Average ILSS-displacement curves under different printing conditions. (Right) Cross-sectional optical micrographs showing the details of the failure modes for the different configurations.

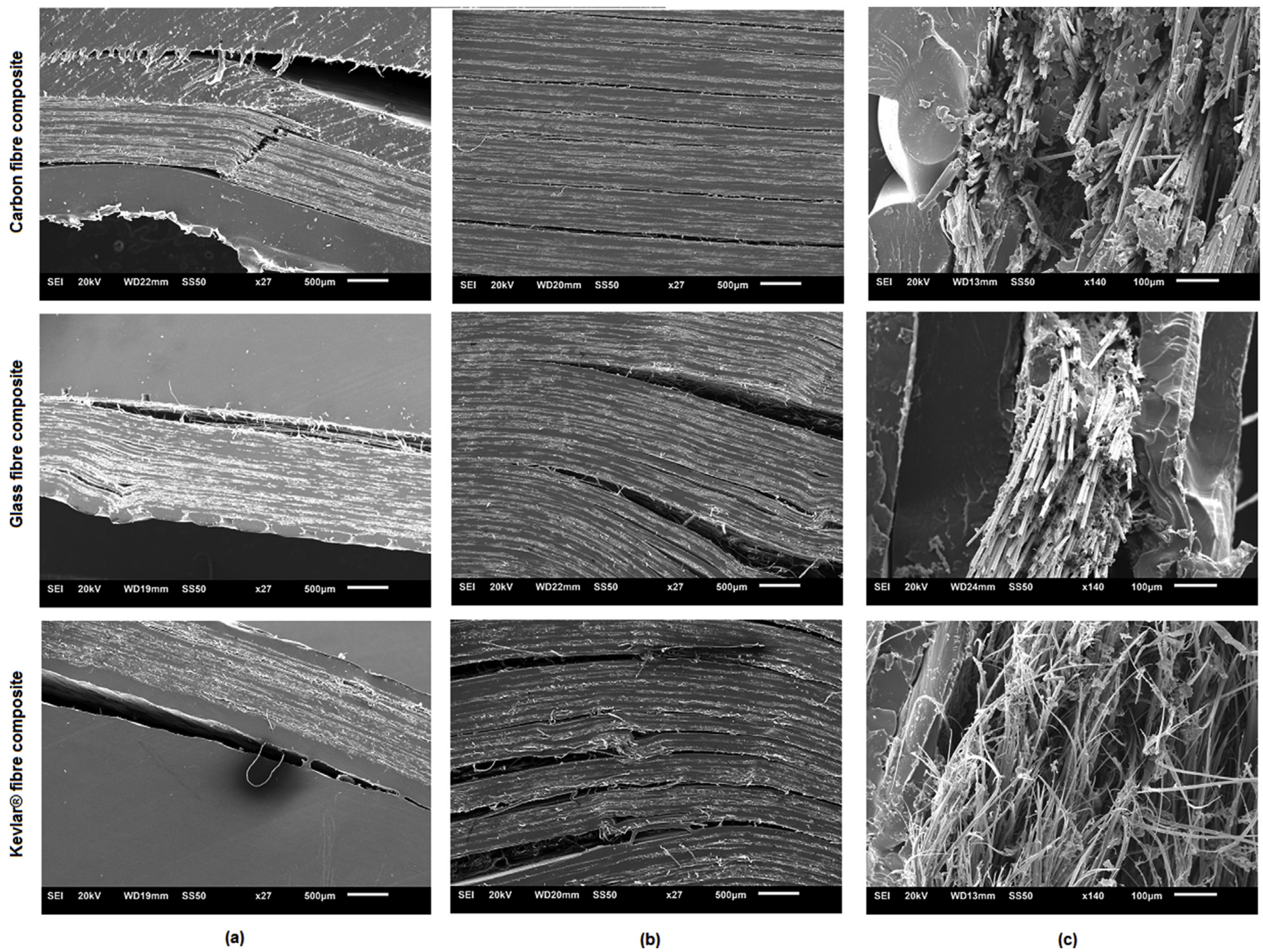

Fig. 5. SEM images showing details of the fractured surfaces of ILSS reinforced samples: (a) Failure modes of type A (x27) and (b) failure modes of type B (x27) ILSS samples. (c) Details of the interface fibre/nylon on fractured surfaces (x140).

3D printed continuous reinforced composites greatly improves the usual mechanical performance of traditional 3D printing parts or reinforced with short fibres and particles. Moreover, another advantage of continuous fibre reinforced 3D printing compared to the unreinforced thermoplastic printing is the stability that the fibres give to the parts, reducing and even avoiding the shape distortions that usually appear in 3D printed parts [17].

4. Conclusions

The interlaminar bonding performance of 3D printed continuous fibre reinforced thermoplastic composites was studied. Continuous glass, carbon and Kevlar® fibres reinforced nylon composites were manufactured by FDM technology. Short Beam Shear test series were carried out to determine the interlaminar shear strength of the printed specimens following the ISO standard recommendations. Different ranges of two process parameters were analysed: layer thickness of unreinforced samples ($L_t = \{0.1, 0.125, 0.2\}$ mm) and fibre volume fraction (type A and B).

It has shown that the effect of layer thickness of unreinforced samples on the interlaminar bonding performance of nylon specimens was marginally significant. It was observed that ILSS decreased as layer thickness increased due to higher porosity. Furthermore, it is worth noting that significant plastic deformation and ductile behaviour was observed.

The effects of the type of reinforcement and fibre content on the interlaminar bonding performance of reinforced nylon specimens were of particular significance. Carbon fibre reinforced composites exhibited the best interlaminar shear performance with higher stiffness. On the other hand, Kevlar® fibre reinforced composites had the lowest interlaminar shear performance due to extensive delamination. This reduction was mainly due to poor wettability of Kevlar® fibre bundles by the nylon (matrix). In addition, the level of increase in interlaminar shear strength was moderate with continued increase in fibre content, particularly in the case of Kevlar® fibres. This was in part due to weak bonding between the fibre/nylon layers as well as the presence of increased levels of air voids.

The results have shown that it is still a challenge to increase interlaminar shear performance of 3D printed continuous reinforced composite material with respect to the autoclave manufacturing of common pre-preg materials. A compaction stage after the deposition of the filament would be desirable to reduce porosity. Nevertheless, the properties obtained by 3D printed continuous reinforced composites by FDM are significantly higher than the usual 3D FDM thermoplastics.

In conclusion, FDM of continuous reinforced composites seems to be a very promising technology with potential for future development. It is a relatively new technique and there is a lack of experimental data on interlaminar bonding performance of structures manufactured by this process, underscoring the need for further research to improve our understanding of the mechanical behaviour of 3D printed composites [35–37].

Acknowledgements

This research was supported by the Spanish Ministerio de Economía y Competitividad (Plan Nacional de I + D + i), under research grants DPI2016-77715-R and DPI2015-65472-R, co-financed by the ERDF (European Regional Development Fund). I García-Moreno also would like to acknowledge the financial support of the Castilla-La Mancha Government (JCCM) and the ERDF (SBPLY/16/180501/000041).

References

[1] J.M. Chacón, M.A. Caminero, E. García-Plaza, et al., Additive manufacturing of PLA structures using fused deposition modelling: effect of process parameters on mechanical properties and their optimal selection, Mater. Des. 124 (2017) 143–157.
[2] G.W. Melenka, B.K.O. Cheung, J.S. Schofield, et al., Evaluation and prediction of the tensile properties of continuous fiber-reinforced 3D printed structures, Compos. Struct. 153 (2016) 866–875.
[3] W. Gao, Y. Zhang, D. Ramanujan, et al., The status, challenges, and future of additive manufacturing in engineering, Comput. Aided Des. 69 (2015) 65–89.
[4] T. Hofstatter, D.B. Pedersen, G. Tosello, et al., State-of-the-art of fiber-reinforced polymers in additive manufacturing technologies, J. Reinforc. Plast. Compos. 36 (2017) 1061–1073.
[5] P. Parandoush, D. Lin, A review on additive manufacturing of polymer-fiber composites, Compos. Struct. 182 (2017) 36–53.
[6] X. Wang, M. Jiang, Z. Zhou, et al., 3D printing of polymer matrix: a review and prospective, Composites Part B 110 (2017) 442–458.
[7] J.M. Chacón, J.C. Bellido, A. Donoso, Integration of topology optimized designs into CAD/CAM via an IGES translator, Struct. Multidiscip. Optim. 50 (2015) 1115–1125.
[8] A. Donoso, J.C. Bellido, J.M. Chacón, Numerical and analytical method for the design of piezoelectric modal sensors/actuators for shell-type structures, Int. J. Numer. Meth. Eng. 81 (2010) 1700–1712.
[9] J.M. Chacón, F.P. García, M. Papaelias, Railroad inspection based on ACFM employing a non-uniform B-spline approach, Mech. Syst. Signal Process. 42 (2013) 605–617.
[10] F. Ning, W. Cong, Y. Hu, et al., Additive manufacturing of carbon fiber-reinforced plastic composites using fused deposition modeling: effects of process parameters on tensile properties, J. Compos. Mater. 28 (2016) 1–12.
[11] A. Lanzotti, M. Grasso, G. Staiano, et al., The impact of process parameters on mechanical properties of parts fabricated in PLA with an open-source 3D printer, Rapid Prototyp. J. 21 (2015) 604–617.
[12] R. Zou, Y. Xia, S. Liu, et al., Isotropic and anisotropic elasticity and yielding of 3D printed material, Composites Part B 99 (2016) 506–513.
[13] J. Kotlinski, Mechanical properties of commercial rapid prototyping materials, Rapid Prototyp. J. 20 (2014) 499–510.
[14] S.S. Yao, F.L. Jin, K.Y. Rhee, et al., Recent advances in carbon-fiber-reinforced thermoplastic composites: a review, Composites Part B 142 (2018) 241–250 https://doi.org/10.1016/j.compositesb.2017.12.007.
[15] A.N. Dickson, J.N. Barry, K.A. McDonnell, et al., Fabrication of continuous carbon, glass and Kevlar fibre reinforced polymer composites using additive manufacturing, Additive Manufacturing 16 (2017) 146–152.
[16] Y. Nakagawa, K.I. Mori, T. Maeno, 3D printing of carbon fibre-reinforced plastic parts, Int. J. Adv. Manuf. Technol. 91 (2017) 2811–2817.
[17] J. Justo, K. Tavara, L. García-Guzman, et al., Characterization of 3D printed long fibre reinforced composites, Compos. Struct. 185 (2018) 537–548.
[18] N. Aliheidari, R. Tripuranenia, A. Ameli, et al., Fracture resistance measurement of fused deposition modeling 3D printed polymers, Polym. Test. 60 (2017) 94–101.
[19] Y. Song, Y. Li, W. Song, et al., Measurements of the mechanical response of unidirectional 3D-printed PLA, Mater. Des. 123 (2017) 154–164.
[20] W. Wu, P. Geng, G. Li, et al., Influence of layer thickness and raster angle on the mechanical properties of 3D-printed PEEK and a comparative mechanical study between PEEK and ABS, Materials 8 (2015) 5834–5846.
[21] C. Yang, X. Tian, D. Li, et al., Influence of thermal processing conditions in 3D printing on the crystallinity and mechanical properties of PEEK material, J. Mater. Process. Technol. 248 (2017) 1–7.
[22] R.J. Zaldivar, D.B. Witkin, T. McLouth, et al., Influence of processing and orientation print effects on the mechanical and thermal behaviour of 3D-printed ULTEM 9085 material, Additive Manufacturing 13 (2017) 71–80.
[23] S. Berretta, R. Davies, Y.T. Shyng, et al., Fused deposition modelling of high temperature polymers: exploring CNT PEEK composites, Polym. Test. 63 (2017) 251–262.
[24] F. van der Klift, Y. Koga, A. Todoroki, et al., 3D printing of continuous carbon fibre reinforced thermo-plastic CFRTP tensile test specimens, Open J. Compos. Mater. 6 (2016) 18–27.
[25] R. Matsuzaki, M. Ueda, M. Namiki, et al., Three dimensional printing of continuous fibre composites by in-nozzle impregnation, Sci. Rep. 6 (2016) 23058.
[26] H.L. Tekinalp, V. Kunc, G.M. Velez-Garcia, et al., Highly oriented carbon fiber-polymer composites via additive manufacturing, Compos. Sci. Technol. 105 (2014) 144–150.
[27] M. Ivey, G.W. Melenka, J.P. Carey, et al., Characterizing short-fiber-reinforced composites produced using additive manufacturing, Adv. Manuf. Polym. Compos. Sci. 3 (2017) 81–91.
[28] R.T. Luiz-Ferreira, I. Cardoso-Amatte, T. Assis-Dutra, et al., Experimental characterization and micrography of 3D printed PLA and PLA reinforced with short carbon fibers, Composites Part B 124 (2017) 88–100.
[29] F. Ning, W. Cong, J. Qiu, et al., Additive manufacturing of carbon fiber reinforced thermoplastic composites using fused deposition modelling, Composites Part B 80 (2015) 369–378.
[30] P. Bettini, G. Alitta, G. Sala, et al., Fused deposition technique for continuous fiber reinforced thermoplastic, J. Mater. Eng. Perform. 26 (2017) 843–848.
[31] X. Tian, T. Liu, C. Yang, et al., Interface and performance of 3D printed continuous carbon fiber reinforce of PLA composites, Composites Part A 88 (2016) 198–205.
[32] C. Yang, X. Tian, T. Liu, et al., 3D printing for continuous fiber reinforced thermoplastic composites: mechanism and performance, Rapid Prototyp. J. 23 (2017) 209–215.
[33] Z. Li, A. Haigh, C. Soutis, et al., Detection and evaluation of damage in aircraft composites using electromagnetically coupled inductors, Compos. Struct. 140 (2016) 252–261.
[34] MarkForged, MarkForged MarkTwo, (2018) https://markforged.com/.
[35] W. Zhang, C. Cotton, J. Sun, et al., Interfacial bonding strength of short carbon fiber/acrylonitrile-butadiene-styrene composites fabricated by fused deposition modelling, Composites Part B 137 (2018) 51–59.
[36] M.S. Islam, P. Prabhakar, Interlaminar strengthening of multidirectional laminates using polymer additive manufacturing, Mater. Des. 133 (2017) 332–339.
[37] P. Parandoush, L. Tucker, C. Zhou, et al., Laser assisted additive manufacturing of continuous fiber renforced thermoplastic composites, Mater. Des. 131 (2017) 186–195.
[38] ISO 14130, Fibre-Reinforced Plastic Composites. Determination of Apparent Interlaminar Shear Strength by Short-Beam Method, (1997).
[39] M. Fernández-Vicente, W. Calle, S. Ferrandiz, et al., Effect of infill parameters on tensile mechanical behaviour in desktop 3D printing, 3D Print. Addit. Manuf. 3 (2016) 183–192.
[40] M.A. Caminero, G.P. Rodríguez, V. Muñoz, Effect of stacking sequence on Charpy impact and flexural damage behaviour of composite laminates, Compos. Struct. 136 (2016) 345–357.
[41] M.A. Caminero, I. García-Moreno, G.P. Rodríguez, Damage resistance of carbon fibre reinforced epoxy laminates subjected to low velocity impact: effect of laminate thickness and ply stacking sequence, Polym. Test. 63 (2017) 530–541.
[42] M.A. Caminero, I. García-Moreno, G.P. Rodríguez, Experimental study of the influence of thickness and ply-stacking sequence on the compression after impact strength of carbon fibre reinforced epoxy laminates, Polym. Test. 66 (2018) 360–370.